Journal of Applied Physics

Electrical, optical, and magnetic properties of Sn doped α-Ga_2O_3 thin films

Cite as: J. Appl. Phys. **120**, 025109 (2016); https://doi.org/10.1063/1.4958860
Submitted: 25 March 2016 . Accepted: 03 July 2016 . Published Online: 14 July 2016

E. Chikoidze, H. J. von Bardeleben, K. Akaiwa, E. Shigematsu, K. Kaneko, S. Fujita, and Y. Dumont

JOURNAL OF APPLIED PHYSICS **120**, 025109 (2016)

Electrical, optical, and magnetic properties of Sn doped α-Ga_2O_3 thin films

E. Chikoidze,[1,a)] H. J. von Bardeleben,[2] K. Akaiwa,[3] E. Shigematsu,[3] K. Kaneko,[3] S. Fujita,[3] and Y. Dumont[1]

[1]*Groupe d'Etude de la Matière Condensée (GEMaC), Université de Versailles Saint Quentin–CNRS, Université Paris-Saclay, 45Av. des Etats-Unis, 78035 Versailles Cedex, France*
[2]*Sorbonne Universités, UPMC Université Paris 6, Institut des Nanosciences de Paris, CNRS, 4, place Jussieu, 75005 Paris, France*
[3]*Department of Electronic Science and Engineering, Kyoto University, Kyoto 615-8510, Japan*

(Received 25 March 2016; accepted 3 July 2016; published online 14 July 2016)

We investigated the effect of Sn doping on the optical, electrical, and magneto transport properties of epitaxial α-Ga_2O_3 thin films grown by mist-Chemical Vapour Deposition. Sn introduces a shallow donor level at ∼0.1 eV and has a high solubility allowing doping up to $10^{20}\,cm^{-3}$. The lowest obtained resistivity of the films is $2.0 \times 10^{-1}\,\Omega$ cm. The Sn doped films with a direct band gap of 5.1 eV remain transparent in the visible and UV range. The electrical conduction mechanism and magneto-transport have been investigated for carrier concentrations below and above the insulator-metal transition. The magnetic properties of the neutral Sn donor and the conduction electrons have been studied by electron spin resonance spectroscopy. A spin $S = 1/2$ state and C_{3V} point symmetry of the neutral Sn donor is found to be in good agreement with the model of a simple Sn_{Ga} center. *Published by AIP Publishing.* [http://dx.doi.org/10.1063/1.4958860]

I. INTRODUCTION

Ga_2O_3 is a wide band gap semiconductor which occurs in different polymorphs (α,β,ε,δ,γ).[1] The poly-type β-Ga_2O_3, which is the stable form of Ga_2O_3 from room temperature up to its melting point, has been studied in the past for its interesting optical and electrical properties: transparency in the deep ultraviolet (UV) and high n-type conductivity.[2] Recently, β-Ga_2O_3 has again become the object of intense research as it has been shown to be of high technological interest as a transparent oxide which has given rise to successful realization of microelectronic devices such as transparent field-effect transistors, high power devices, photodetectors, and photodiodes.[3–7] From the viewpoint of fabricating corundum-structured alloys for band gap engineering, α phase Ga_2O_3 is very appealing. The stabilisation of the α-phase, which crystallizes in the corundum structure (Figure 1(a)), can be obtained by heteroepitaxy of thin films on Al_2O_3.[8]

In the corundum structure, the distance between Ga^{+3} ions are considerably shorter than in the monoclinic β-phase.[9] The oxygen ions are approximately hexagonal close packed and gallium ions occupy two-thirds of the octahedral sites. The band structure of α-Ga_2O_3 with rhombohedral $R\bar{3}c$ symmetry has been calculated by He *et al.*[10] It was shown that in comparison to β-type, α-Ga_2O_3 might have a higher band gap, refractive index, and reflectance but a lower effective mass of electrons.

This work focuses on the study of the properties of n-type α-Ga_2O_3 obtained by the mist chemical vapour deposition (mist-CVD) growth technique.[11] It has been reported before that Ga_2O_3 oxide can be rendered n-type by Sn and Si doping.[12–14] We investigate the transport, optical, and magnetic properties of highly Sn-doped epitaxial layers, below and above the insulator to metal transition (I/M). We show that it is possible to grow high quality Sn-doped α-Ga_2O_3 μm thin films on c-plane sapphire (c-Al_2O_3) and control the n-type conductivity by Sn incorporation during the growth. We have investigated the optical transparency in the visible (VIS) and UV region and the electronic and magneto-transport properties of the films with Sn concentration ranging from 10^{18} to $1 \times 10^{20}\,cm^{-3}$. We performed Electron Spin Resonance (ESR) measurements on the neutral donor and conduction electron spin systems, which coexist in the highly doped samples.

II. EXPERIMENTAL PROCEDURE

Epitaxial films were grown by the mist chemical vapour deposition (mist-CVD) method on c-Al_2O_3 substrates. Gallium(III) acetylacetonate and tin(II) chloride dihydrate were chosen as gallium and tin precursors, respectively. These precursors, dissolved in water with the addition of a small amount of hydrochloric acid, were used as the reaction source. The concentration of the gallium precursor was fixed at 0.05 mol/l. The growth temperature was 500 °C. Molecular nitrogen was used as a carrier gas. To obtain different carrier concentrations the tin precursor concentration in the source was varied between 0.05% and 0.4%. In the source solution, the oxidation state of Sn ion is 2+, because $SnCl_2$ was used as a Sn source, but, in the Ga_2O_3 film, Sn probably occurs in a 4+ state. In forming process of Ga_2O_3 material, water from the source solution plays two roles: first, it acts as an oxygen source, and second, it acts as an oxidation reagent—reducing the Sn 2+ ion into a 4+ state. From secondary ion mass spectroscopy (SIMS) analyses, it was found that Sn concentrations in the samples (A, B, C, D, and E*) vary from 1×10^{18} to $1 \times 10^{20}\,cm^{-3}$. The thickness of the layers d varies between

a)Author to whom correspondence should be addressed. Electronic mail: ekaterine.chikoidze@uvsq.fr

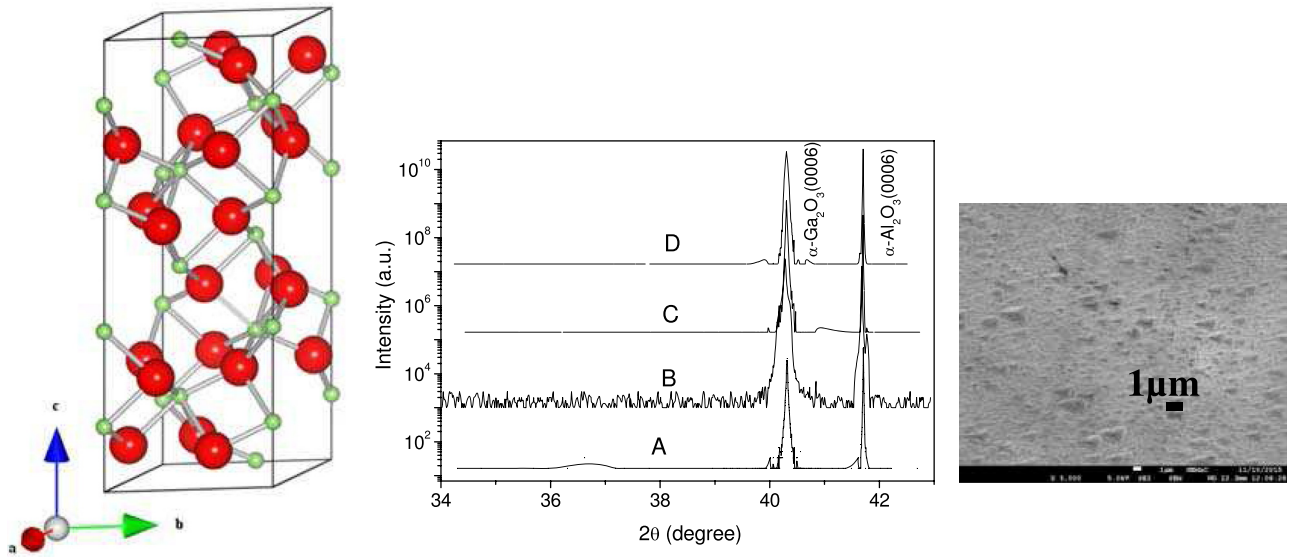

FIG. 1. (a) Rhombohedral $R\bar{3}c$ crystal structure of α-Ga_2O_3, with small (green) Ga atoms and big (red) O atoms. (b) Cu $_{K\alpha}$ X-ray diffraction $2\theta - \theta$ scans profiles for samples A, B, C, and D. (c) SEM image of sample B.

600 nm and 2400 nm. X-ray diffraction (XRD) patterns were obtained with an ATX Rigaku X-ray diffractometer. Figure 1(b) shows the 2θ-θ scans for four samples with increasing doping levels. All samples showed the (0006) diffraction peak of α-Ga_2O_3 and did not show any peaks related to other phase. A broadening of the diffraction peak with increasing doping level was attributed to increasing strain.[10]

Figure 1(c) presents an image (acquired on a JEOL JSM 7001F scanning electron microscope (SEM)) of sample B; the relatively flat surface confirms the 2D growth mechanism. From atomic force microscopy (AFM), the surface roughness (root-mean squared) was estimated to be around 0.6 nm.

The optical properties of the films were investigated with a Perkin-Elmer UV–VIS–near infrared (NIR) spectrophotometer at room temperature.

The electrical contacts for highly conducting Sn doped samples were prepared by indium soldering, while for lowest doped samples O and A, Ti/Au contacts were deposited by RF-sputtering. As verified by I-V measurements, all contacts showed an Ohmic behaviour. DC-resistivity and magnetoresistance (MR) for the samples B, C, D, and E* were studied with a commercial "DC-resistivity" configuration in a 9T-PPMS (Quantum Design, Inc.) environment, while for highly resistant (sample resistance > 1 MΩ) samples O and A, a home-designed high impedance measurement set-up was used. Magneto-resistance was measured with a magnetic field applied perpendicular to the film plane. Hall effect measurements were performed in the van der Pauw configuration for magnetic fields (perpendicular to the film plane) varying up to 1.6 T. Seebeck effect measurements were carried out with a home-made system built combining a Keithley SCS-4200 with Kelvin probes from cascade Microtech.

Electron Spin Resonance (ESR) measurements were performed with a Bruker X-band spectrometer under standard conditions: 100 kHz field modulation and low (μW) microwave power in order to avoid nuclear polarization effects. The samples were studied in the temperature range of T = 4 K to T = 295 K.

III. EXPERIMENTAL RESULTS AND DISCUSSION

A. Electrical transport and optical properties

α-Ga_2O_3 is a wide band gap material, and the un-doped sample O should be highly resistive, if it is not contaminated with impurities. Indeed, this sample showed a relatively high resistivity ($\rho = 4 \times 10^5$ Ω cm) at room temperature resistivity. Previously, a deviation from stoichiometry and, in particular, oxygen vacancies has been invoked to explain the high n-type conductivity observed in nominally undoped Ga_2O_3 bulk crystals. However, this hypothesis seems to be questionable, as recent hybrid functional calculations predict the oxygen vacancy to be a deep donor with an ionization energy higher than 1 eV.[15] As shown in Table I, Sn doping drastically decreases the room temperature ρ: for sample *A*, we obtain $\rho = 1.3 \times 10^1\,\Omega\,\mathrm{cm}$ compared to $\rho = 4.1 \times 10^5\,\Omega\,\mathrm{cm}$ for the undoped sample. The ρ decreases further with increasing doping levels (sample *B* and *C*), then diminishes slightly when the dopant concentration reaches $N_D = 2 \times 10^{19}\,\mathrm{cm}^{-3}$ (sample *D*), and then returns to a higher value, $N_D = 1 \times 10^{20}\,\mathrm{cm}^{-3}$, for sample E*, which is similar to the case of β-Ga_2O_3.[16] Sn

TABLE I. Sample names, Sn percentage in the source during the deposition, Sn concentration in the samples measured by SIMS, and room temperature ρ measured in the van der Pauw configuration.

Sample	Sn in the source (%)	[Sn] (cm^{-3})	$\mathrm{Rho}_{300\,K}$ (Ω cm)
O	0	0	2.1×10^5
A	0.005	1.0×10^{18}	1.3×10^1
B	0.02	2.0×10^{18}	1.2×10^0
C	0.05	4.6×10^{18}	1.3×10^{-1}
D	0.1	1.6×10^{19}	2.0×10^{-1}
E*	0.4	1.0×10^{20}	2.5×10^0

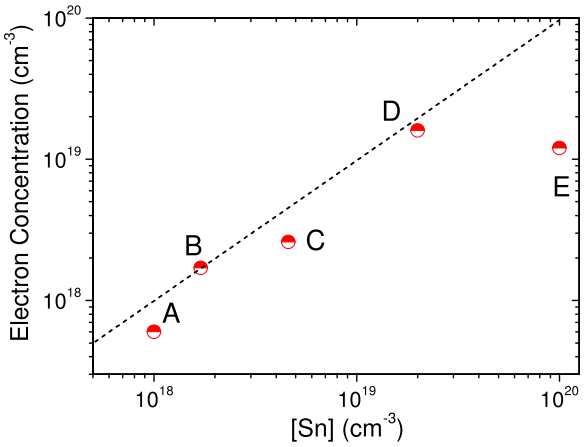

FIG. 2. Room temperature electron concentrations, determined from Hall Effect versus Sn content measured by SIMS for samples *A*, *B*, *C*, *D*, and E. The black line is the theoretical "total ionisation" line of Sn.

is expected to substitute for Ga^{3+} and introduce a single donor state $D^{0/+}$ due to its electron configuration $5s^2 5p^2$.

The sign of the conductivity type was checked by Seebeck Effect measurements in the 300–400 K temperature range. From the measurement of the temperatures difference and of the associated voltage difference, the Seebeck coefficient S, defined as $S = \delta V/\delta T$, was determined to be $-100\,\mu V/K$ at 310 K for sample C; this value is very similar to those reported for the Sn doped β-Ga_2O_3.[7]

A further confirmation of the n-type conductivity was obtained from Hall Effect measurements which gave the negative sign for the majority carriers for all the Sn-doped samples. The free carrier concentrations determined by Hall Effect measurements at 300 K versus Sn dopant concentration measured by SIMS are plotted in Figure 2. The carrier density (n) changes linearly with Sn incorporation, from $n = 6 \times 10^{17}\,cm^{-3}$ to $n = 1.6 \times 10^{19}\,cm^{-3}$ for samples A, B, C, and D. For sample E*, with the highest doping level (of $[Sn] = 10^{20}\,cm^{-3}$), the value of n concentration does not increase. This doping level can be considered as a solubility limit.

The temperature dependence of ρ was measured in order to investigate the electrical transport mechanism. With increasing ion of incorporated Sn concentration, it was expected that there would be the thermally activated conductivity to the conduction band (CB) due to ionization of the Sn dopant, followed by donor impurity band formation and finally metallic conduction above the doping level given by the Mott criterion.[17] The Mott metal–insulator transition occurs at a dopant critical concentration N_{Mott}, when $N_{Mott}^{1/3} a_B \approx 0.27$,[18] where a_B is an impurity Bohr radius. The donor Bohr radius in β-Ga_2O_3 was reported as $a_B = 1.8$ nm,[19] assuming a similar value for the Sn donor in α-Ga_2O_3, the Mott transition is expected to occur for a donor concentration $N_{Mott} \approx 4 \times 10^{18}\,cm^{-3}$. The impurity band creation depends not only on the impurity Bohr radius but also on the degree of compensation, however. In this regime, the ρ might show a "metallic" like behaviour, i.e., it does not change significantly when the temperature is lowered below 300 K. For high doping levels with $N_D > N_{Mott}$, the impurity band is expected to broaden and finally merge with the CB; in this case of a degenerate semiconductor, the Fermi level is in the CB. The condition for degenerate doping is $N_D^{-1/3} \approx a_B$, which for Ga_2O_3:Sn should occur for $N_{Sn} \approx 1 \times 10^{20}\,cm^{-3}$.

For sample *B*, with $[Sn] = 2.0 \times 10^{18}\,cm^{-3} < N_{Mott}$, a room temperature ρ of 1.2 Ω cm was measured. An *n* of $1.4 \times 10^{18}\,cm^{-3}$ and a mobility (μ) of $= 3.2\,cm^2/V\,s$ were deduced.

Figure 3 shows the temperature dependence of ρ and σ for samples B, C, and D. Two temperature regions can be clearly distinguished for samples B and C: $T < 170$ K and $T > 170$ K. The high temperature part corresponds to thermal carrier activation to the CB, while the low temperature part is related to impurity band conduction.[20,21] For sample B, a thermal activation energy of $E_1 = 100$ meV is found. In the low temperature region (the impurity conduction regime) ρ varies as

$$\rho = \rho_3 \exp(\varepsilon_3/k_B T), \tag{1}$$

where k_B is Boltzmann constant, T the temperature, and ε_3 is a hopping activation energy with values in the meV range.[20] Indeed, a fit of the low temperature part according to Eq. (1) gives a value of $\varepsilon_3 = 0.2$ meV. A particular feature of the impurity band conduction is the high sensitivity to a small change in doping level. Indeed, a comparison with sample *C* (which has twice the higher Sn concentration) shows that the ρ decreases by more than an order to magnitude to give $\rho = 0.13\,\Omega$ cm at room temperature. The Sn concentration [Sn] in sample *C* is $4.6 \times 10^{18}\,cm^{-3}$, which is about the value for which an insulator to metal transition is expected, and indeed, the resistivity changes very insignificantly for $T > 250$ K. (Figure 3(a)). The activation energy in the higher temperature region is $E_I = 8$ meV, indicating that conduction occurs in an impurity band. Whereas n increased to $2.6 \times 10^{18}\,cm^{-3}$ the μ

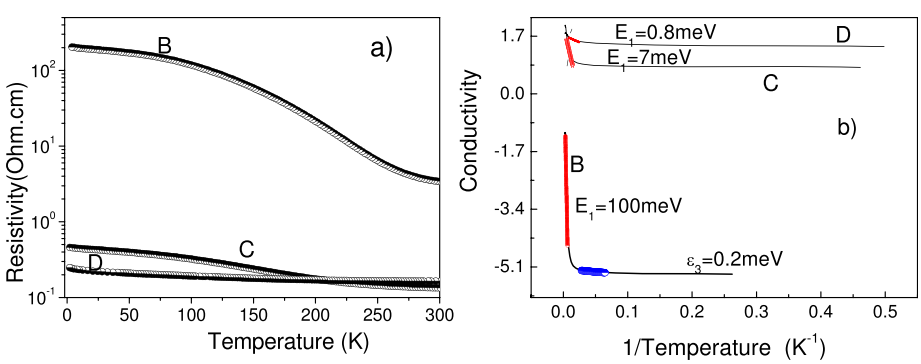

FIG. 3. (a) Electrical resistivity versus temperature for samples B, C, and D; (b) logarithm of electrical conductivity versus 1/temperature. E_1 band activation energies of 100 meV, 7 meV and 0.8 meV are determined from the high temperature region (red linear fits) and $E_3 = 0.2$ meV is deduced for impurity band conduction for sample B (blue linear fit).

mobility decreases to 2.1 cm^2/V s, due to increased impurity scattering.

With higher doping in sample *D*, [Sn] = $2.0 \times 10^{19}\,cm^{-3}$, at 300 K, we obtain the following values: $\rho = 0.2\,\Omega\,cm$, $n = 1.6 \times 10^{19}\,cm^{-3}$, and $\mu = 1.9\,cm^2$/V s. A similar low μ for high doping levels was also reported for β-Sn:Ga_2O_3.[22] Sample *D* is in the $N_D > N_{Mott}$ regime, above the I-M transition, but with $N_D < N_c$ ($N_c \approx 3 \times 10^{19}\,cm^{-3}$), i.e., not yet degenerate. The ρ shows a pronounced metallic behaviour (Figure 3(a)).

The band gap of undoped α-Ga_2O_3 was previously reported to be 5.3 eV.[8] Optical transmittance and reflectance were conducted in the 200–3000 nm wavelength range for samples *A*, *B*, *C*, and *D*. All samples were transparent in the visible (VIS) and near infrared (NIR) spectral regions. Optical transmittance in the deep ultraviolet (UV) (for 250 nm photons) varies from 76% to 38% depending on the doping level (Figure 4(a)). Transparency decreased for sample D, with $N_D > N_{Mott}$ being in the regime above the I-M transition. Transmittance in NIR spectral region significantly decreases for D sample due to the higher concentration of charge carriers (Figure 4(a) inset).

From the analysis of the optical transmittance and reflectance data, the character (direct or indirect) and the value of the optical band gap can be evaluated.[23] Indeed, for a direct band gap, $\alpha(h\nu) \sim \frac{\sqrt{h\nu - E_g}}{h\nu}$ and for an indirect band gap, $\alpha(h\nu) \sim \frac{(h\nu - E_g)^2}{h\nu}$, with h$\nu$ equal to the incident photon energy, $\alpha(h\nu)$ the optical absorption coefficient, and E_g the optical band gap. Consequently, $(h\nu\alpha)^2 \sim h\nu - E_g$ and $\sqrt{h\nu\alpha} \sim h\nu - E_g$, respectively. Plotting $\alpha(h\nu)^2$ and $\sqrt{\alpha h\nu}$ as a function of photon energy hν, clear direct band gap dependences are found (see, for example, the inset of Figure 4(b) for the highest doped sample (D)). Sn-doped α-Ga_2O_3 showed a direct band-gap material up to doping levels of $2.0 \times 10^{19}\,cm^{-3}$ (Figure 4(b)). For the optical gap, a value of $E_g = 5.16$ eV was obtained at 300 K, independent of the dopant concentration for samples A, B, and C. A slight decrease to $E_g = 5.11$ eV occurs for sample D. This is not as would be expected for the Burstein-Moss shift, i.e., the increase in band gap due to the occupied lowest CB states. This shift, ΔE_g, is proportional to the $n^{2/3}$ and inversely proportional to the effective mass of the carriers.[24] But the Burstein-Moss effect occurs only in degenerate semiconductors (as was observed for degenerate β-Ga_2O_3),[7] which is not the case in our samples.

B. Magneto-transport

The temperature dependent magnetoresistance of α-Sn:Ga_2O_3 films was measured. The Magnetoresistance MR (in %) is defined as

$$MR = \frac{R(B) - R(B=0)}{R(B=0)} \times 100\%, \tag{2}$$

where $R(B)$ is the résistance measured for a magnetic field, B, applied perpendicular to the applied current. For sample A, no reliable results could be obtained due to the high resistance and associated high noise level; only the positive sign (increase of resistance with magnetic field) of the magnetoresistance could be determined.

For sample *B* with [Sn] < N_{Mott}, the results at T = 2 K, 10 K, and 50 K are given in Figure 5(a). At T = 2 K, a strong positive MR was observed, with a value of 7% at 9 T. With increasing temperature, *MR* decreases and becomes negligible at 50 K. The low temperature positive magneto-resistance is characteristic of hopping conduction, which is typical for moderately doped non-magnetic semiconductors.[25,26] It can be attributed to a competition between two processes: electron-donor (*e-d*) interaction and electron-electron (*e-e*) interaction. In the case of non-degenerate materials, the first interaction dominates; the magnetic field compresses the electronic wavefunction for the donor and thus reduces the thermally activated carrier concentration, which increases the resistance.[27] This effect occurs when the magnetic field is perpendicular to the current plane, since, in this configuration, the magnetic field gives rise to an additional "magnetic" potential (oscillator potential) $\frac{\hbar^2 r^2}{8m^* \lambda^4}$, where λ is a magnetic length given by $\lambda = \left[\frac{\hbar^2 c}{eH^2}\right]^{1/2}$, m^* is the effective electron mass, $r = \sqrt{x^2 + y^2}$ the radius of the circular electronic orbit in the plane perpendicular to the *z*-axis, *c* the speed of light, *e* the electron charge of electron, and $\hbar$ the reduced Planck constant.[28] At low magnetic fields (B = μ_0H < 1 T), a signature of weak negative MR is observed. This indicates that the *e-e* interaction at this doping level starts to be non-negligible.

For sample *C*, close to the IM transition, the MR effect is important below 10 K, when impurity band conduction

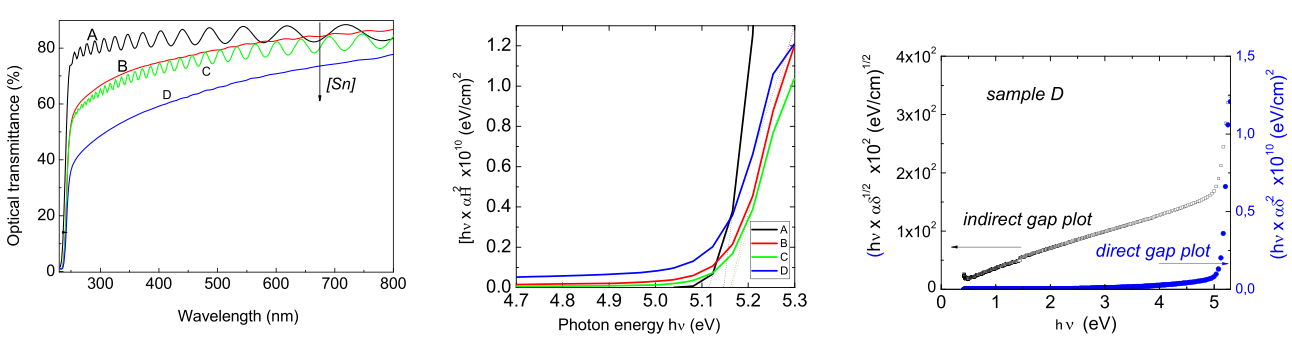

FIG. 4. (a) Optical transmittance of Sn doped α-Ga_2O_3 as a function of photon wavelength for samples A, B, C, and D; (b) optical direct gap determination for samples from the absorption coefficient α (c) direct and indirect band gap corresponding plots for sample D.

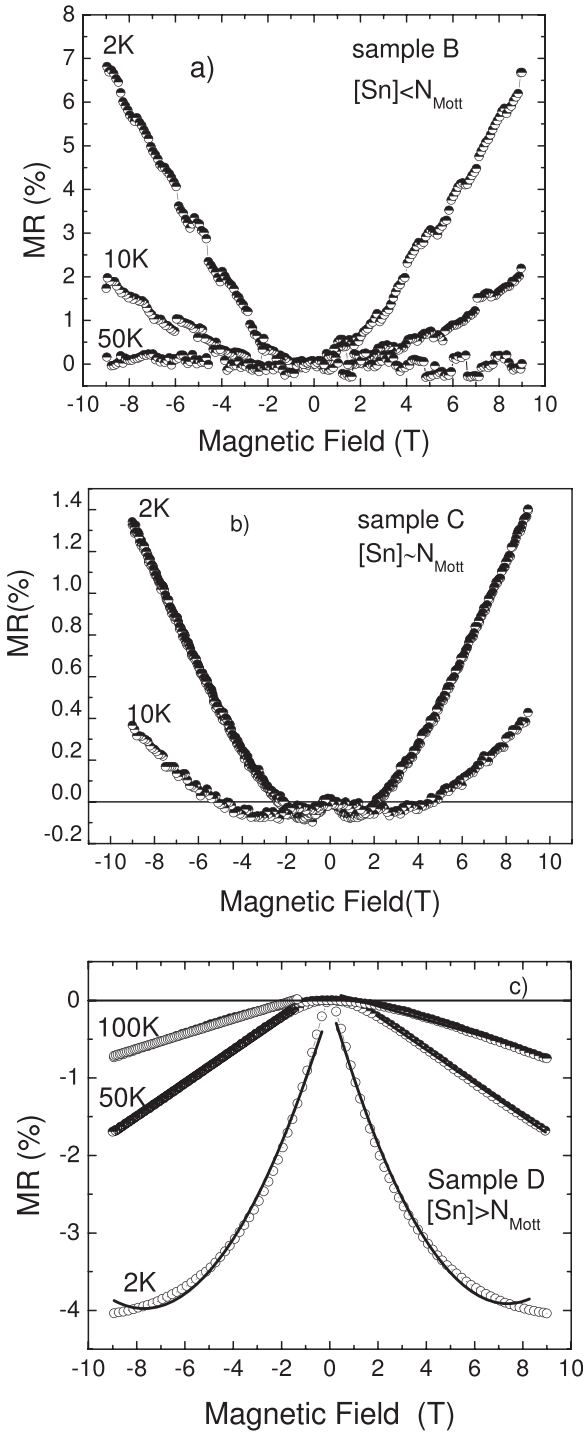

FIG. 5. Magneto-resistance at different temperatures in perpendicular magnetic field configuration for: (a) sample B $[Sn] < N_{Mott}$; (b) magneto-resistance at different temperatures in perpendicular magnetic field configuration for sample C, $[Sn] \approx N_{Mott}$; (c) magneto-resistance at different temperatures in perpendicular magnetic field configuration for sample D $[Sn] > N_{Mott}$. The black lines are fits. Magnetic field is perpendicular to applied current.

occurs (Figure 5(b)). We see that the MR is small in magnitude (1.3% for 9 T at 2 K) and changes sign: it is positive at high magnetic field ($B > 1$ T) and negative at lower fields. Indeed, when impurity wavefunctions overlap, the *e-e* interaction starts to be stronger. It was reported by several authors that the MR for highly doped semiconductors may be divided into two terms: a negative and a positive component, the strength of which depends on the external magnetic field.[26,29,30]

The positive MR has a linear dependence on the square root of the applied magnetic field.[30] Plotting MR versus $B^{1/2}$ (high field) for samples B and C, a linear dependence is indeed observed (Figures 6(a) and 6(b)). The magnitude of the cross-over field B_{cross}, where the MR changes sign from negative to positive, is a function of the carrier density and temperature. The increasing temperature B_{cross} shifts to higher values.[29] This behavior is observed for sample C (Figure 6(b)), for which the crossover field shifts from B $\approx$ 1.7 T to B $\approx$ 3 T when the temperature is increased from 2 K to 10 K.

For the sample *D*, which is above the I-M transition with $N_D > N_{Mott}$, the MR is negative for all temperatures from 2 K up to 100 K. The value of MR = 4% at 2 K for $B = 9$ T. Negative MR has been theoretically predicted and later observed in non-magnetic materials with impurity hopping conduction; it is attributed to the formation of localized magnetic moments of the impurity electrons.[31] The negative MR varies with a Curie-Weiss type dependence on the magnetic field and temperature:[25] $MR = -\beta \frac{B}{T+\theta}$, where β is a proportionality coefficient. Indeed, it was observed (Figure 5(c)) that at 50 K and 100 K MR(B) varies linearly with the applied field B. At the lowest temperature of 2 K, the conduction mechanism changes to variable range hopping. Then, the conduction proceeds via the tunnelling of electrons between donor states. In the impurity conduction regime, most of the donors have localized magnetic moments, which interact with the delocalized electrons. With the applied magnetic field, the magnetic moments become aligned and the probability of intrinsic scattering decreases, leading to an increase in conductivity (MR < 0). The saturation of the negative MR, which we observe at 2 K, has been explained by Sasaki as being due to the saturation of the magnetization.[32] The magnetic properties of the donor system can also be studied by ESR spectroscopy.

C. ESR spectroscopy

ESR spectroscopy is a technique well suited for the study of both neutral shallow donors, as well as electrons in the CB. The two systems can be distinguished by ESR, in particular, since their type of magnetism differs. The magnetism of free electrons is a Pauli-type paramagnetism, which is independent of temperature. Whereas donor bound electrons show a Curie- or Curie-Weiss-type behaviour, with ESR intensity proportional to $\frac{1}{T-\theta}$, where θ is the Curie-Weiss temperature. Further, the principal values of the g-tensor will be different even though the values for effective mass like donors and CB will be rather similar. If a central hyperfine interaction can be observed, this is another element to distinguish the two systems. In the case of high doping levels, i.e., of sample B, there will be a more complicated, mixed situation with the simultaneous presence of bound and free electrons, the relative contributions of which will depend on the temperature.

The line shape of the donor resonance and its variation with temperature give equally important information of the

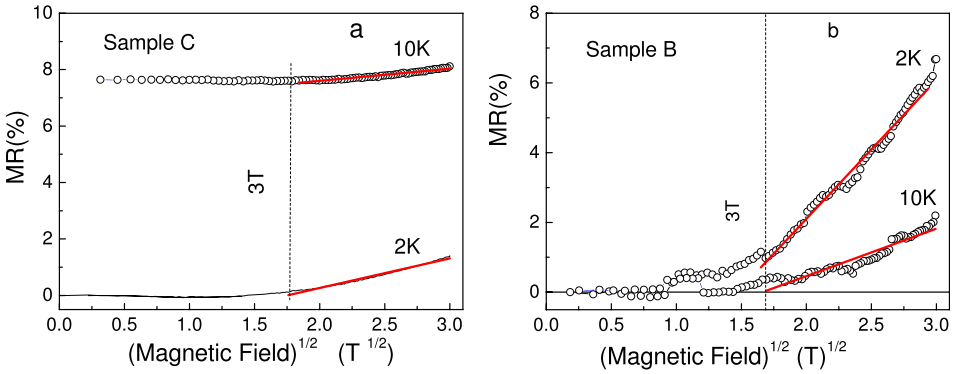

FIG. 6. (a) Magneto-resistance plotted versus square root of applied magnetic field at 2 K and 10 K for sample B. Continuous lines are linear fits for $3 \leq \mu_0 H \leq 9T$ range. (b) Magneto-resistance plotted versus square root of applied magnetic field at 2 K and 10 K for sample C. Red continuous lines are linear fits for $3 \leq \mu_0 H \leq 9T$ range.

localized/non-localized character of the paramagnetic donors and possible exchange interactions. In the simplest case, of localized neutral donors, the ESR line shape is expected to be Gaussian due to inhomogeneous broadening from the hyperfine interaction with the dominant (^{69}Ga, ^{71}Ga) nuclear spins, which have a high nuclear moment and 100% I = 3/2 spin states. For an isolated neutral donor in Ga_2O_3, a linewidth of $\sim 10^2$ G would be expected whereas motional narrowing and exchange interactions will reduce this linewidth dramatically.

The following focuses on sample B ([Sn] $< N_{Mott}$), which is characteristic for this series of samples. The electrical transport measurements can be used to associate the observed ESR spectra with donors in the impurity band, or free electrons in the conduction band. They show two main temperature regions (T > 170 K and T < 170 K) in which thermal emission to the CB and hopping conductivity in an impurity band prevail, respectively. Clearly, this picture is schematic because both electrons in an impurity band and free electrons coexist in an intermediate temperature range.[33]

Figure 7 shows EPR spectra obtained for the orientation of the magnetic field B//c at T = 295 K and 4 K. All samples show a single line spectrum, the intensity of which scales with [Sn] for the samples B, C, and D. The line shape is Lorentzian rather than Gaussian, which implies that motional narrowing and exchange narrowing effects average out the hyperfine interactions. The Lorentzian line profile persists even at low temperature (T = 4 K), which shows that, in sample B, rather than being localized, the donor electrons are delocalized in an impurity band with thermally activated hopping conduction. Furthermore, the linewidth of only $\Delta Bpp \approx 1$ G is much smaller than would be expected for localized donors but agrees with the conclusion of the transport measurements which indicated the formation of an impurity band and thermal emission to the CB, respectively.

The single line spectrum corresponds to a spin S = 1/2 system, as expected for a neutral, single donor or a free electron in the CB. The site symmetry of the donor can be obtained from the symmetry of the g-tensor determined from the angular variation of the ESR spectra for rotation of the magnetic field in the c-plane and perpendicular to this plane (Figure 8). The results show an axial symmetry (C_{3v}) with two principal g-factor values—g//c and g⊥c—as expected for free CB electrons in the α-Ga_2O_3 corundum structure.

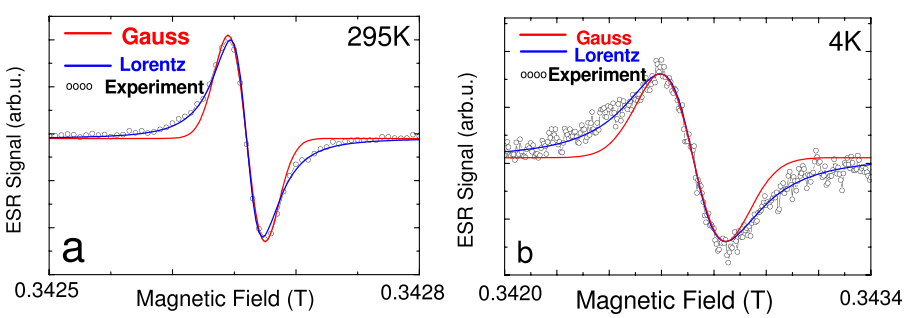

FIG. 7. (a) ESR spectrum of sample B at T = 295 K and for B//c; (b) ESR spectrum of sample B at T = 4 K and for B//c. Data (circles) are adjusted with Gaussian fit (red) and Lorentzian fit (blue).

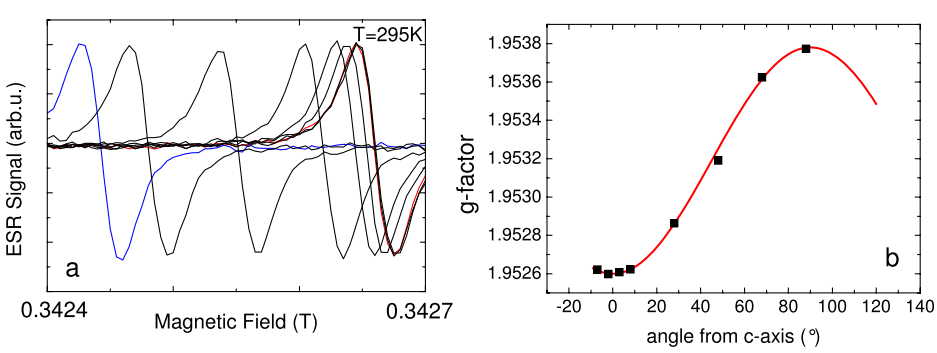

FIG. 8. (a) ESR spectra for different orientations of the magnetic field between B//c and B⊥c at T = 295 K; (b) angular variation of the g-factor for a rotation of the magnetic field between B//c and B⊥c at T = 295 K; red line is simulation, and squares are experimental points.

TABLE II. Principal values of the g-tensor and linewidths for sample B and Sn doped β-Ga_2O_3; T = 295 K and T = 4 K.

	g-tensor $T = 295$ K	ΔB_{pp}(G) $T = 295$ K	g-tensor $T = 4$ K	ΔB_{pp}(G) T = 4 K	Reference
α- Sn:Ga_2O_3	$g_{xx} = g_{yy} = 1.9538$	0.3	$g_{xx} = g_{yy} = 1.9536$	2.3	This work
"sample B"	$g_{zz} = g//c = 1.9526$		g_{zz}=g//c = 1.9525		
β- Sn:Ga_2O_3	$g_{xx} = 1.960$	1.0			34
	$g_{yy} = 1.958$				
	$g_{zz} = 1.962$				

The general spin Hamiltonian for a neutral donor with spin S = 1/2 is

$$H = -\mu_B\ \vec{B}\bar{\bar{g}}\vec{S} + A\,\vec{S}.\vec{I} + \vec{S}\bar{\bar{T}}\vec{I},$$

where μ_B is the Bohr magneton, $\bar{\bar{g}}$ the Landé g-tensor, $\vec{B}$ the applied magnetic field, $\vec{S}$ the electron angular momentum, A the central hyperfine interaction constant, $\vec{I}$ the nuclear angular momentum, and $\bar{\bar{T}}$ the super-hyperfine interaction tensor. Due to the delocalized character of the donor, the central hyperfine interactions with the Sn nucleus and the super-hyperfine interaction with the surrounding Ga nuclei are averaged out, and only the g-tensor anisotropy can be observed.

Table II shows the g-values obtained at T = 295 K and T = 4 K and compares them to the previously studied case of a shallow donor in β-Ga_2O_3. As the crystal symmetry of β-Ga_2O_3 is lower (orthorhombic), the g-tensor for a substitutional donor Sn_{Ga} has equally lower symmetry. The point symmetry of the ESR spectrum at T = 4 K, where donor bound electrons are measured, is unchanged and in good agreement with the model of Sn being a Ga site substitutional single donor.

The g-values of *CB* electrons can be calculated in the *k-p* model, which requires the knowledge of the energies of the lowest *CB*s and the spin-orbit splitting of *VB* and *CB*. In the case of wurtzite GaN, for example, an average g-value of g = 1.95 was obtained,[35] in good agreement with experimental results. In the case of α-Ga_2O_3 and β-Ga_2O_3, these values are not available.

Whereas the g-tensor of shallow donors is generally temperature independent, this is not the case in sample B. As shown in Figure 9, the g-factor g//c decreases linearly with

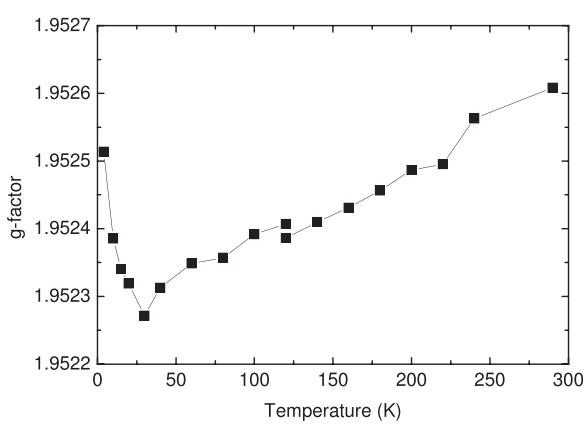

FIG. 9. Variation with temperature of the g-factor for B//c.

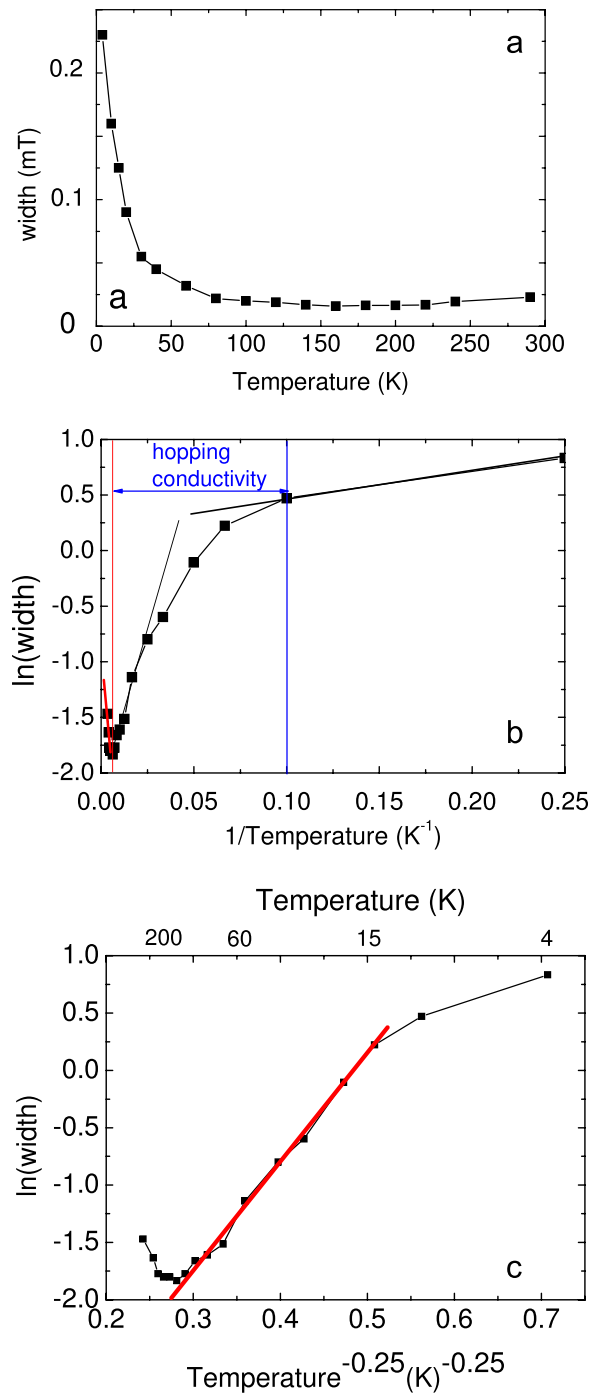

FIG. 10. (a) Variation with temperature of the ESR linewidth for B//c; (b) ln(width) versus 1/temperature; and (c) ln(width) versus $T^{-0.25}$.

temperature until 30 K. Below T = 30 K, it increases again but with a much higher slope. The same behaviour is observed for the g⊥c value. If it is essentially free electrons that are observed at room temperature and only donor bound electrons at T = 4 K, then that their g-values are indeed very close.

A similar behaviour is observed as for the g-factors: a small decrease in the temperature range 295 K to 50 K and strong increase at lower temperatures. The linewidth variation within the two conduction states model was analysed. Figure 10 shows the linewidth ΔB_{pp} as a function of temperature.

Figure 10(b) shows the ln(width) versus 1/temperature. The variation is well described by this dependence in the high temperature region and in the very low temperature region, where thermal activation to the CB and to the excited donor states takes place, respectively. In the intermediate region, the variation of the linewidth cannot be described by this exponential variation. However, plotting the linewidth as ln(width) as a function of $T^{-0.25}$, the variation expected for variable range hopping reproduces nicely its variation (Figure 10(c)).

The temperature dependence of the ESR signal intensity was also analysed by a double integration of the experimental spectra. The results (Figure 11) show that we have two distinct temperature regions: (i) high temperature 295 K to 50 K with a temperature independent ESR intensity and (ii) a low temperature region, T < 50 K, where Curie like behaviour becomes dominant.

IV. CONCLUSION

The electrical transport properties of highly Sn doped α-Ga_2O_3 thin films were investigated. It was found that with [Sn] between 10^{17} and $-10^{19}\,cm^{-3}$, semiconducting and metallic n-type conductive behaviors can be obtained, without significantly modifying the optical transparency in the visible or UV region. The $\alpha-$phase has an advantage in doping efficiency with respect to the well studied β-phase of gallium oxide, due to having only one possible octahedral site of Ga in the corundum structure.[36] Electrical and magneto-transport studies revealed several conduction regimes: below, close, and above the M-I transition. ESR spectroscopy showed that the spin S = 1/2 state and C_{3V} point symmetry of the neutral Sn donor are in good agreement with the model of a simple Sn_{Ga} center. α-Ga_2O_3 is a large band gap semiconductor similarly to diamond (Eg = 5.3 eV), but with much higher efficiency of doping capability, and availability as a low-cost and 4 inch size single crystalline substrate from FLOSFIA, Inc, Japan. In 2016 firstly was demonstrated α-Ga_2O_3 based schottky barrier diode with parameters close to SiC based one.[37] All the above indicate that α-Ga_2O_3 oxide has remarkable potential for "transparent electronics" and high-power/voltage applications.

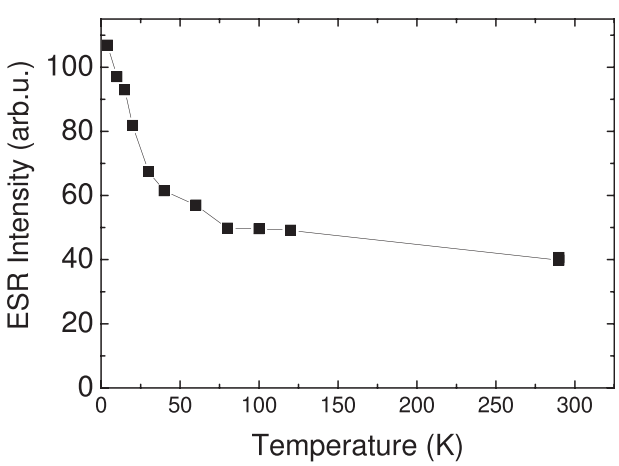

FIG. 11. Variation with temperature of the ESR intensity obtained by double integration.

ACKNOWLEDGMENTS

We express our thanks to French Embassy in Japan, for financially supporting E. Shigematsu during his stay in the GEMaC laboratory, France. We also acknowledge B. Berini for the preparation of metallic contacts, C. Vilar for providing SEM images, and G. Bouchez for technical support in carrying out optical measurements.

[1]R. Roy, V. G. Hill, and E. F. Osborn, J. Am. Chem. Soc. **74**, 719 (1952).
[2]H. H. Tippins, Phys. Rev. **140**, A316 (1965).
[3]K. Matsuaki, H. Hiramatsu, K. Nomura, H. Yanagi, T. Kamiya, M. Hirano, and H. Hosono, Thin Solid Films **496**, 37 (2006).
[4]M. Higashiwaki, K. Sasaki, A. Kuramata, T. Masui, and S. Yamakoshi, Appl. Phys. Lett. **100**, 013504 (2012).
[5]M. Zhong, Zh. Wei, X. Meng, F. Wu, and J. Li, J. Alloys Compd. **619**, 572 (2015).
[6]S. Nakagomi, T. Momo, S. Takahashio, and Y. Kokubun, Appl. Phys. Lett. **103**, 072105 (2013).
[7]N. Ueda, H. Hosono, R. Waseda, and H. Kawazoe, Appl. Phys. Lett. **70**, 3561 (1997).
[8]D. Shinohara and S. Fujita, Jpn. J. Appl. Phys., Part 1 **47**, 7311 (2008).
[9]S. Geller, J. Chem. Phys. **33**, 676 (1960).
[10]H. He, R. Orlando, M. A. Blanco, R. Pandey, E. Amzallag, I. Baraille, and M. Rérat, Phys. Rev. B **74**, 195123 (2006).
[11]K. Akaiwa and S. Fujita, Jpn. J. Appl. Phys., Part 1 **51**, 070203 (2012).
[12]T. Kawaharamura, G. T. Dang, and M. Furuta, Jpn. J. Appl. Phys., Part 1 **51**, 040207 (2012).
[13]N. Suzuki, S. Ohira, M. Tanaka, T. Sugawara, K. Nakajima, and T. Shishido, Phys. Status Solidi C **4**, 2310 (2007).
[14]T. Oshima, K. Matsuyama, K. Yoshimatsu, and A. Ohtomo, J. Cryst. Growth **421**, 23 (2015).
[15]J. B. Varley, J. R. Weber, A. Janotti, and C. G. Van de Walle, Appl. Phys. Lett. **97**, 142106 (2010).
[16]W. Mi, X. Du, C. Luan, H. Xiao, and J. Ma, RSC Adv. **4**, 30579 (2014).
[17]B. L. Bonch-Bruevich and S. G. Klashnikov, *The Physics of Semiconductors* (Nauka, Moscow, 1990), p. 677.
[18]N. F. Mott and E. A. Davis, *Electronic Properties of Noncrystalline Materials* (Clarendon Press, Oxford, 1979), p. 590.
[19]Y. P. Song, H. Z. Zhang, C. Lin, Y. W. Zhu, G. H. Li, F. H. Yang, and D. P. Yu, Phys. Rev. B **69**, 075304 (2004).
[20]F. Mott and W. D. Twose, Adv. Phys. **10**, 107 (1961).
[21]A. Miller and E. Abrahams, Phys. Rev. **120**, 745 (1960).
[22]M. Orita, H. Ohta, and H. Hosono, Appl. Phys. Lett. **77**, 4166 (2000).
[23]I. Pankove, *Optical Processes in Semiconductors*, 2nd ed. (Dover, New York, 1975).
[24]E. Burstein, Phys. Rev. **93**, 632 (1954).
[25]L. Halbo and R. J. Sladek, Phys. Rev. **173**, 794 (1968).
[26]W. Kraak, U. Troppenz, R. Herrmann, S. M. Chudinov, and V. A. Kulbachinskii, Phys. Status Solidi B **148**, 333 (1988).
[27]S. Ishida, Physica E **18**, 294 (2003).
[28]A. Bottger and V. V. Bryskin, *Hopping Conduction in Solids* (Wiley-VCH Verlag GmbH, Berlin, 1985), p. 398.
[29]P. Kuivalainen, J. Heleskivi, M. Leppihalme, U. Gyllenberg-Gastrin, and H. Isotalo, Phys. Rev. B **26**, 2041 (1982).

[30]T. F. Rosenbaum, R. F. Milligan, M. A. Paalanen, G. A. Thomas, R. N. Bhatt, and W. Lin, Phys. Rev. B **27**, 7509 (1983).
[31]Y. Toyozawa, J. Phys. Soc. Jpn. **17**, 986 (1962).
[32]W. Sasaki, J. Phys. Soc. Jpn. **20**, 825 (1965).
[33]D. V. Savchenko, E. N. Kalabukhova, A. Po, E. N. Mokhov, and B. D. Shanina, Phys. Status Solidi B **248**, 2950 (2011).
[34]M. Yamaga, E. G. Víllora, K. Shimamura, N. Ichinose, and M. Honda, Phys. Rev. B **68**, 155207 (2003).
[35]W. E. Carlos, J. A. Freitas, Jr., M. Asif Khan, D. T. Olson, and J. N. Kuznia, Phys. Rev. B **48**, 17878 (1993).
[36]S. C. Siah, R. E. Brandt, K. Lim, L. T. Schelhas, R. Jaramillo, M. D. Heinemann, D. Chua, J. Wright, J. D. Pekins, C. U. Segre, R. G. Gordon, M. F. Toney, and T. Buonassi, Appl. Phys. Lett. **107**, 252103 (2015).
[37]M. Oda, R. Tokuda, H. Kambara, T. Tanikawa, T. Sasaki, and T. Hitora, Appl. Phys. Express **9**, 021101 (2016).